

Life Cycle of Superfluid Vortices and Quantum Turbulence in the Unitary Fermi Gas

Gabriel Wlazłowski,^{1,2,*} Aurel Bulgac,^{2,†} Michael McNeil Forbes,^{3,4,2,‡} and Kenneth J. Roche^{5,2,§}

¹*Faculty of Physics, Warsaw University of Technology, Ulica Koszykowa 75, 00-662 Warsaw, Poland*

²*Department of Physics, University of Washington, Seattle, Washington 98195-1560, USA*

³*Department of Physics & Astronomy, Washington State University, Pullman, Washington 99164-2814, USA*

⁴*Institute for Nuclear Theory, University of Washington, Seattle, Washington 98195-1550, USA*

⁵*Pacific Northwest National Laboratory, Richland, Washington 99352, USA*

(Dated: Tuesday 22nd July, 2014)

The unitary Fermi gas (UFG) offers an unique opportunity to study quantum turbulence both experimentally and theoretically in a strongly interacting fermionic superfluid. It yields to accurate and controlled experiments, and admits the only dynamical microscopic description via time-dependent density functional theory (DFT) – apart from dilute bosonic gases – of the crossing and reconnection of superfluid vortex lines conjectured by Feynman in 1955 to be at the origin of quantum turbulence in superfluids at zero temperature. We demonstrate how various vortex configurations can be generated by using well established experimental techniques: laser stirring and phase imprinting. New imaging techniques demonstrated by the MIT group [Ku *et al.* arXiv:1402.7052] should be able to directly visualize these crossings and reconnections in greater detail than performed so far in liquid helium. We demonstrate the critical role played by the geometry of the trap in the formation and dynamics of a vortex in the UFG and how laser stirring and phase imprint can be used to create vortex tangles with clear signatures of the onset of quantum turbulence.

PACS numbers: 67.85.Lm, 67.85.De, 03.75.Ss, 03.75.Kk, 67.85.-d, 05.30.Fk,

Quantized vortices are a hallmark of superfluids. Their generation, dynamics, evolution, and eventual decay have been studied experimentally and theoretically for some six decades in liquid ⁴He and ³He, Bose and Fermi cold atom systems, neutron stars, condensed matter systems, cosmology, and particle physics. The two-component unitary Fermi gas (UFG) is of particular interest due to precise experimental control in cold atom traps, and almost direct applicability to dilute matter in neutron star crusts where experiments and direct observations are not possible. The experimental control and universality of the system make it one of enormous interest for those studying phenomena in relativistic heavy-ion collision, nuclear physics, nuclear astrophysics, atomic physics, and condensed matter physics.

In a recent letter [1], we showed that the initial conditions as described in the MIT experiment [2] – which claimed to have an axially symmetric trap – lead to the production of superfluid vortex rings. The properties of these rings provided a natural explanation of several puzzling characteristics displayed by the objects observed in [2] which they called “heavy solitons”. In particular, the vortex ring scenario explained successfully the long oscillation periods, the unusually large apparent effective mass of the objects, and details of the imaging procedure that resulted in objects appearing much larger than the natural width of a vortex.

The experiment [2] was recently updated [3] with an improved method of imaging slices from the original ex-

periment (tomography), conclusively demonstrating that the “heavy solitons” are ultimately vortex segments that consistently align themselves across the vertical imaging axis. The authors of [3] suggest that this systematic alignment is due to asymmetries in the trap arising from gravitational distortions of the optical trapping potential in the vertical direction.

The optical trapping potential in the x and y directions is an axially symmetric gaussian altered by gravity in the vertical direction y :

$$V(x, y, z) = \frac{m\omega_z^2 z^2}{2} + \mathcal{O}(z^4) + V_0 \left[1 - \exp \left(-\frac{m\omega_x^2 (x^2 + y^2)}{2V_0} \right) \right] + mgy. \quad (1)$$

Shifting $y \rightarrow y + y_0$ where y_0 is the new minimum gives the following effective trapping potential

$$V(x, y + y_0, z) \approx \frac{m\omega_z^2 z^2}{2} + \mathcal{O}(z^4) + \frac{m\omega_x^2 x^2}{2} + \frac{m\omega_y^2 y^2}{2} + Cy^3 + \mathcal{O}(\delta^2) + \text{const} \quad (2)$$

where $\delta = 3mg^2/4\omega_x^2 V_0$ is treated perturbatively, and

$$\omega_y \approx \omega_x (1 - \delta), \quad C \approx \frac{2m\omega_x^4}{3g}\delta. \quad (3)$$

According to [3], $\delta = 1 - \omega_y/\omega_x \approx 5\%$ is small, justifying this expansion. The axial symmetry is thus broken by two effects: an anisotropy δ and an anharmonicity Cy^3 which we characterize in terms of $C_0 = m\omega_y^2/2R$ where $C = C_0$ would give equal quadratic and cubic terms at the

* gabrielw@if.pw.edu.pl

† bulgac@uw.edu

‡ mforbes@alum.mit.edu

§ k8r@u.washington.edu

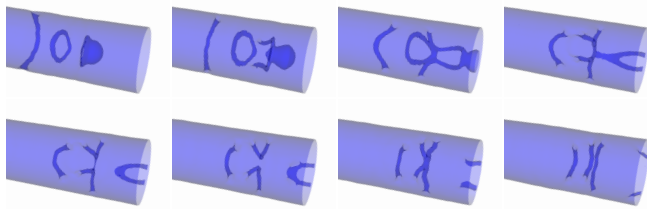


FIG. 1. (Color online, click on frames to view movie online.) Demonstration of off-axis vortices in the UFG generated by firing a “bullet” along an axially symmetric trap in a movie [9] from Ref. [6]. Off-axis vortex rings attach to the walls, and turn into vortex lines that cross and reconnect. The movie [9] also demonstrates that vortex rings and lines move at similar velocities.

Thomas-Fermi (TF) radius R where $V(0, R + y_0, 0) = \mu$. With the experimental parameters [2, 3], $C/C_0 \approx \delta \approx 5\%$.

Here we show that accounting for gravity indeed induces the initially produced vortex rings [1, 4, 5] to convert into vortex lines, which oscillate along the long axis of the trap. The conversion of off-axis vortex rings into vortex lines on the boundary of a trap was first demonstrated in the UFG in the simulations of [6] (reproduced in Fig. 1). In the context of [2], the possibility of this conversion was also suggested in Ref. [7], where asymmetries were induced manually through stochastic noise. Without a systematic asymmetry in the trap, however, stochastic variations lead to randomly orientated vortex lines inconsistent with the experimental observations. The simulations [7] model only the condensate, but lack averaging over stochastic trajectories or a density matrix as required to properly describe thermal fluctuations. The role of these fluctuations also diminishes at low temperatures, becoming irrelevant at zero temperature. Our zero-temperature approximation is supported by [8] which finds thermal effects to be negligible for vortex reconnection.

Gravity provides a systematic breaking of the axial symmetry, allowing for a consistent conversion of the initial vortex rings into a horizontally oriented vortex line, though the exact nature of this conversion seems to be quite sensitive to geometry. A similar sensitivity to geometry was noted in both experiment [10] and theory [6] where a high degree of axial symmetry was found to be critical in the formation and stability of a vortex lattice. As can be seen in [6] (see the movie [9]), [7], and the simulations presented here, vortex rings and vortices move with almost the same velocity. This is to be expected since small segments of both vortex rings or vortex lines move according to the well established Magnus relationship in response to a similar buoyant force directed out from the trap (see [11] for a discussion and references therein). Both large rings and vortices have the same structure and core depletion, and will therefore move with comparable velocities and periods up to small corrections due to geometric (curvature) effects.

Likewise, the expansion of a large vortex ring and a vortex segment will behave similarly, so the subtle de-

pendence of the final image on the imaging procedure as discussed in [1] remains valid, explaining how the vortex core of the inter-particle scale expands to appear as a much larger object. The only potentially noticeable difference between the motion of vortex rings and vortices is a possible asymmetry in the oscillations for vortex rings which return as a small ring down the centre of the trap. It turns out, however, that the asymmetry in this motion is quite small except in the case of very large amplitude oscillations [1, 12]. As a result, distinguishing between the two scenarios is best performed by imaging from different directions or through tomography [3].

Here we extend the fermionic superfluid local density approximation (SLDA) simulations of [1] to include an anisotropy δ and anharmonicity C/C_0 to model the dynamics of an imprinted domain wall in a cloud of ~ 560 particles in the UFG. We use the same formalism and initial state preparation detailed in [1] on a $32^2 \times 128$ lattice, but now include gravitational effects (2) comparable to those describing the trap in [3].

While our simulations only contain about a thousand particles, they provide a more accurate representation of the initial experimental conditions than available through any other technique. In particular, the extended Thomas-Fermi (ETF) model – a bosonic Gross-Pitaevskii equation (GPE)-like density functional theory (DFT) – used in [1, 4, 5] lacks a mechanisms for the superfluid to relax. Thus, while suitable for studying the qualitative dynamics of vortex motion in large traps, the ETF is not suitable for the period shortly after the imprint where the system exhibits significant relaxation (see the supplemental material [13] for a comparison between the SLDA and the ETF). An *ad hoc* relaxation was included in Ref. [7], but this model does not reproduce UFG equation of state, and lacks the quantitative validation of the SLDA where the functional is fully determined by fitting quantum Monte Carlo (QMC) and experimental results (see [14] and references therein). Despite the absence of an explicit collision integral, the large number of degrees of freedom in the SLDA permit many mechanisms for superfluid relaxation including various phonon processes, Cooper pair breaking, and Landau damping.

We start in Fig. 2 with a moderate anisotropy $\delta \approx 10\%$ which elongates the trap vertically as in the experiment. As demonstrated in [1], the phase imprint rapidly seeds the formation of a vortex ring, but as this ring evolves, it is attracted to the surface and eventually hits the nearer boundaries on the side, converting to a pair of vortex lines. These lines then oscillate along the trap undergoing a crossing and recombination process similar to that seen using GPE simulations [15] – the mechanism responsible for quantum turbulence – changing orientation from horizontal to vertical and back. The addition of a $C/C_0 \approx 3\%$ anharmonicity along the y direction, similar to that induced by gravity in the experiment, breaks the mirror symmetry, and one of the two vortices is gradually ejected from the system, leaving a single vortex oriented horizontally along the shorter axis of the trap that oscillates

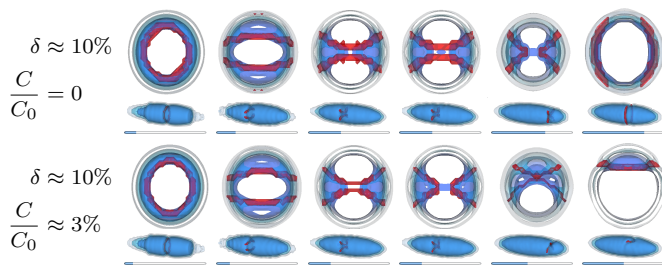


FIG. 2. (Color online, click on frames to view movie online.) Effects of moderate anisotropy $\delta = 1 - \omega_y/\omega_x \approx 10\%$ (trap is taller than wide): the ring hits the narrow walls on the side, forming two parallel vortices. Without any anharmonicity $C = 0$ (top), these undergo several recombinations, oscillating between a horizontal and vertical orientation. The presence of an anharmonicity $C/C_0 \approx 3\%$ breaks the symmetry, eventually expelling one vortex from the system, resulting in a long-lived vortex that oscillates back and forth.

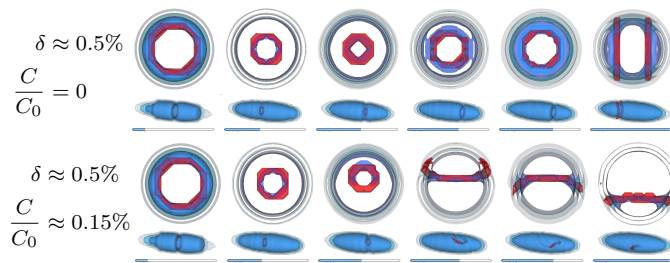


FIG. 3. (Color online, click on frames to view movie online.) Effects of weak anisotropy: the ring now lives long enough to return as a small ring. Without an anharmonicity (top) several oscillations occur before the ring expands and hits the walls forming two parallel vortices. Adding a weak anharmonicity (bottom) causes the small ring to rotate. Once twisted off axis, this ring rapidly converts to a single vortex as seen in [7]. The rapid production of a single vortex from a twisted defect was also described in [16] and provides a convenient way of constructing vortices.

through the cloud, consistent with the observations [3].

In Fig. 3 we compare similar systems, but now with asymmetries an order of magnitude smaller. In this case, the vortex ring persists much longer before converting into vortex lines, long enough to return as a small vortex down the centre of the trap. This smaller vortex appears to be very sensitive to even a tiny anharmonicity which causes it to tilt upwards and collide with the upper wall of the trap, rapidly forming a single horizontally aligned vortex. This rapid formation of a single vortex from a tilted ring or imprint was also obtained in simulation [7] and mentioned in [3, 16], and seems like a more reliable mechanism for consistently forming a single horizontally aligned vortex (see the movie tilted imprint in the supplemental material [17]).

In particular, as demonstrated in the top of Fig. 4, even when given a negative anisotropy $\delta \approx -10\%$ so that the trap is compressed vertically, a meta-stable horizontally aligned vortex may still result. It was suggested in [3]

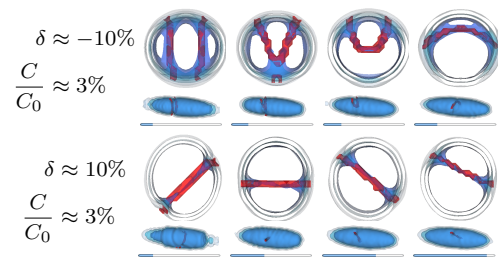


FIG. 4. (Color online, click on frames to view movie online.) The trap on the top is wider than it is tall – the energetically favored configuration would be a vertical vortex, but the initial conditions lead to a slightly more energetic vortex aligned along the longer of the two axes. On the bottom, we imprint an oblique vortex line in a trap with the same asymmetry as the experiment. As it oscillates long the trap, the vortex alignment oscillates about the favored horizontal position, but without significant damping, continues past this alignment to another oblique position. The presence of significant damping – such as through phonons at finite T – might allow this to relax to a horizontal alignment. However this relaxation would likely be comparable to the time it takes the vortex to oscillate out of the system – the true “minimum” energy state has no vortex at all.

that the horizontal alignment results from the fact that this state has lower energy, but evolution in these systems is conservative to a high degree of accuracy, hence rapid progress toward a state with lower energy or larger statistical weight is not guaranteed a priori. Indeed, a lower energy state exists – that with the vortex ejected from the system – and we expect the timescale for a vortex to relax into a stable horizontal configuration to be comparable to or longer than the timescale for a vortex to lose its energy and completely oscillate out of the system. To check, we imprinted a misaligned vortex in a trap with both asymmetries $\delta \approx 10\%$ and $C/C_0 \approx 3\%$. As shown on the bottom of Fig. 4, although this vortex does rotate toward the horizontal configuration, it quickly rotates past the configuration to an approximate mirror misalignment.

While here we have stressed the role of broken symmetries in the evolution of vortex rings, it is still a challenge for experimentalists to perform similar experiments in axially symmetric traps, similar to those used in [10], where vortex rings are likely to survive for long periods of time.

Almost six decades ago, Feynman [18] envisioned vortex crossing and recombination as responsible for quantum turbulence in cold superfluids which lack dissipation at zero temperature. While many study turbulent phenomena [19–25], we are aware of a few recent experiments that have directly observed in experiment the vortex crossing and recombination mechanism [26–29]. These dynamics and interactions play a crucial role in many fermionic superfluids with applications to condensed matter physics, neutron stars, cosmology, particle physics (see e.g. [30]). For example, to explain pulsar glitches in neutron stars, one may need to quantitatively understand energy loss during crossing and recombination as inputs to glitching

models (see e.g. [11]). The UFG provides an almost ideal laboratory study these phenomena and benchmark the SLDA. Using multiple tilted imprints, for example, one can control the generation and arrangement of multiple vortices in order to study collisions, reconnection, and interactions. The UFG and SLDA thus provides a new microscopic framework to study aspects of quantum turbulence in a strongly interacting system, complementing weakly-interacting dilute Bose gases [31, 32] modelled with the GPE as the only microscopic frameworks presently available for studying superfluid dynamics.

The phase imprint technique can be also utilized to create turbulent states with many tangled vortices. Here we demonstrate one approach, adding a phase imprint [2, 3] to a lattice of vortices which can be created experimentally by stirring using laser beams [10]. In Fig. 5 we show consecutive frames of turbulent motion exhibiting crossings and recombinations of quantized vortices in an elongated harmonic trap. The simulation was done in a $48^2 \times 128$ box comprising 1410 fermions (see supplemental material [17] for a movie). We also show the corresponding probability distribution function (PDF) of the velocities for longitudinal v_{\parallel} and transverse v_{\perp} components of the velocity (with respect to long axis).

We start with the ground state of a cloud cut in half with a knife-edge potential. We then stir the system with two circulating laser beams parallel to the long axis of the trap. Once a vortex lattice is generated, we imprint a π phase shift between the halves. Just before removing the edge knife, we introduce a slight tilt to speed the formation of a vortex tangle. After the knife-edge is removed, the vortex lines twist, cross, and reconnect. From the velocity PDFs one sees a clear departure from gaussian behaviour as the tangle evolves – a hallmark of quantum turbulence. Eventually the system relaxes to a vortex lattice and equilibrates in v_{\parallel} . Somewhat similar velocity PDFs are seen in theoretical studies of dilute Bose gases [33] and in phenomenological filament model of the crossing-recombination vortex line dynamics [34].

In conclusion, have shown the crucial role played by the trap geometry in the formation of a vortex line after a phase imprint. In particular we identified a few possible scenarios for the short term evolution of the phase imprint in the experiments [2, 3], showing that the details are highly sensitive to geometric factors. To precisely characterize the behavior realized in the experiments [2, 3], the experiment will likely need to be simulated with precise values of the trapping asymmetries known, and with realistic particle numbers which are currently are beyond the capabilities of the most advanced implementations of the SLDA approach. Satisfactory agreement with the latest MIT experiments serves as the next step in validating the time-dependent SLDA, demonstrating that it is capable of qualitatively describing the complex dynamics of strongly interacting fermionic systems. We have demonstrated that recombination is likely present in the early stages of the experiments [2, 3] (see Figs. 2 and 3) and can be selected for by reducing the anharmonicity of

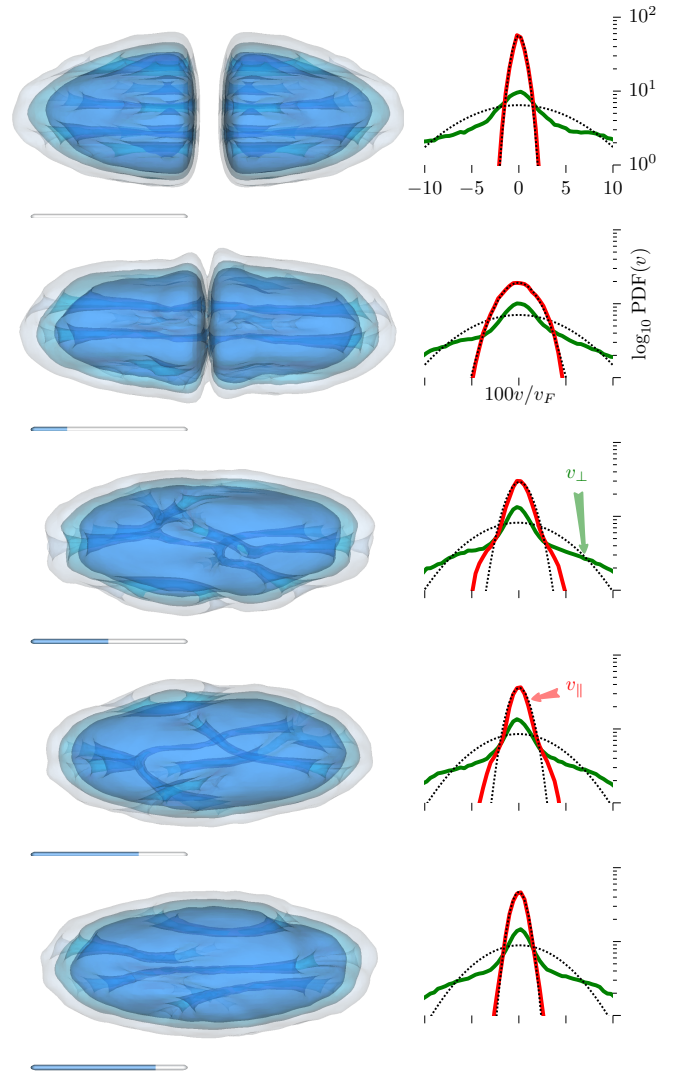


FIG. 5. (Color online, click on frames to view movie online.) Generation of quantum turbulence by phase imprint of the vortex lattice. In the left column consecutive frames show: a) vortex lattice with knife edge dividing cloud, b) just after phase imprint removal of the knife, c-e) decay of turbulent motion. In the right column we show the corresponding PDFs for longitudinal v_{\parallel} and transverse v_{\perp} components of collective velocity. Dotted lines show the gaussian best fit to the data.

the trap. We have also presented that the phase imprint technique can be utilized to generate quantum turbulent state. Therefore, using improved imaging techniques [3] coupled with carefully designed initial conditions, cold atom experiments have a great opportunity to directly probe and quantify the dynamics and interactions vortices and the potential to significantly advance our understanding of quantum turbulence. In this regard, the unitary Fermi gas is of particular interest as the results will have almost direct impact on superfluid dynamics and turbulent phenomena in strongly interacting Fermi superfluids, in particular neutron star phenomenology.

We thank L. Chuek, M. Ku, and M. Zwierlein for

describing details of their experiment. We acknowledge support under U.S. Department of Energy (DoE) Grant No. DE-FG02-97ER41014 and the Polish National Science Center (NCN) grant under decision No. DEC-2013/08/A/ST3/00708. G.W. acknowledges the Center for Advanced Studies at Warsaw University of Technology for the support under Contract No. 58/2013 (international research scholarships financed by the European Union from the European Social Funds, CAS/32/POKL).

MMF acknowledges support from the Institute for Nuclear Theory during the program *Universality in Few-Body Systems: Theoretical Challenges and New Directions, INT-14-1*. Some of the calculations reported here have been performed at the University of Washington Hyak cluster funded by the NSF MRI Grant No. PHY-0922770. This research also used resources of the National Center for Computational Sciences at Oak Ridge National Laboratory [35], which is supported by the Office of Science of the DoE under Contract DE-AC05-00OR22725.

-
- [1] A. Bulgac, M. M. Forbes, M. M. Kelley, K. J. Roche, and G. Wlazłowski, Phys. Rev. Lett. **112**, 025301 (2014), arXiv:1306.4266 [cond-mat.quant-gas].
- [2] T. Yefsah, A. T. Sommer, M. J. H. Ku, L. W. Cheuk, W. Ji, W. S. Bakr, and M. W. Zwierlein, Nature **499**, 426 (2013), arXiv:1302.4736 [cond-mat].
- [3] M. J. H. Ku, W. Ji, B. Mukherjee, E. Guardado-Sanchez, L. W. Cheuk, T. Yefsah, and M. W. Zwierlein, “Motion of a Solitonic Vortex in the BEC-BCS Crossover,” (2014), arXiv:1402.7052.
- [4] M. D. Reichl and E. J. Mueller, Phys. Rev. A **88**, 053626 (2013), arXiv:1309.7012.
- [5] W. Wen, C. Zhao, and X. Ma, Phys. Rev. A **88**, 063621 (2013), arXiv:1309.7408 [cond-mat.quant-gas].
- [6] A. Bulgac, Y.-L. Luo, P. Magierski, K. J. Roche, and Y. Yu, Science **332**, 1288 (2011).
- [7] P. Scherpelz, K. Padavić, A. Rançon, A. Glatz, I. S. Aranson, and K. Levin, “Phase Imprinting in Equilibrating Fermi Gases: The Transience of Vortex Rings and Other Defects,” (2014), arXiv:1401.8267.
- [8] A. J. Allen, S. Zuccher, M. Caliari, N. P. Proukakis, N. G. Parker, and C. F. Barenghi, Phys. Rev. A **90**, 013601 (2014), arXiv:1404.4557.
- [9] <http://www.phys.washington.edu/groups/qmbnt/UFG/ntball-oc-wz.m4v>.
- [10] M. W. Zwierlein, J. R. Abo-Shaeer, A. Schirotzek, C. H. Schunck, and W. Ketterle, Nature **435**, 1047 (2005).
- [11] A. Bulgac, M. M. Forbes, and R. Sharma, Phys. Rev. Lett. **110**, 241102 (2013), arXiv:1302.2172 [nucl-th].
- [12] L. P. Pitaevskii, “Hydrodynamic theory of motion of quantized vortex rings in trapped superfluid gases,” (2013), arXiv:1311.4693.
- [13] See supplementary material at [INCLUDE_LINK_HERE](#) for details about our simulations, comparison of fermionic and bosonic simulations and list of movies..
- [14] A. Bulgac, M. M. Forbes, and P. Magierski, “The Unitary Fermi Gas: From Monte Carlo to Density Functionals,” in *The BCS–BEC Crossover and the Unitary Fermi Gas*, Lecture Notes in Physics, Vol. 836, edited by W. Zwerger (Springer, Berlin Heidelberg, 2012) Chap. 9, pp. 305 – 373, arXiv:1008.3933.
- [15] F. Piazza, L. A. Collins, and A. Smerzi, New J. Phys. **13**, 043008 (2010), arXiv:1011.5041.
- [16] N. Parker, *Numerical Studies of Vortices and Dark Solitons in Atomic Bose-Einstein Condensates*, Ph.D. thesis, University of Durham (2004).
- [17] Movies are provided here: http://www.phys.washington.edu/~bulgac/media_files/VR2 and on YouTube:
- SLDA Movies**
<http://youtu.be/qtxD1VCK-08> (Fig. 1),
<http://youtu.be/Vxv0Ps0s-6s> (Fig. 2t, δ : 10%, C : 0),
<http://youtu.be/7qG03kmN-fs> (Fig. 2b, δ : 10%, C : 3%),
<http://youtu.be/gIfhB7QrGxU> (Fig. 3t, δ : 0.5%, C : 0),
<http://youtu.be/K74GUp1cDnM> (Fig. 3b, δ : 0.5%, C : 0.15%),
<http://youtu.be/0pg8N91-gZ0> (Fig. 4t, δ : -10%, C : 3%),
<http://youtu.be/7xlG15TUNQs> (Fig. 4b, δ : 10%, C : 3%),
http://youtu.be/_aW00tI00dw (tilted imprint),
<http://youtu.be/utpkynynd1Qkc> (colliding vortices),
<http://youtu.be/nCGtq8k6SAQ> (Fig. 5, turbulence),
ETF Movies (corresponding to the listed figures)
<http://youtu.be/uDu00V005D4> (Fig. 2t, δ : 10%, C : 0),
<http://youtu.be/L50NtMQDfgE> (Fig. 2b, δ : 10%, C : 3%),
<http://youtu.be/VUrlvJglqkI> (Fig. 3t, δ : 0.5%, C : 0),
<http://youtu.be/H0IB-R1TwJU> (Fig. 3b, δ : 0.5%, C : 0.15%),
<http://youtu.be/EXL0lBbsKS8> (Fig. 4, δ : -10%, C : 3%).
- [18] R. Feynman, Prog. Low Temp. Phys. Progress in Low Temperature Physics, **1**, 17 (1955).
- [19] W. F. Vinen and J. J. Niemela, J. Low Temp. Phys. **128**, 167 (2002).
- [20] W. F. Vinen, J. Low Temp. Phys. **145**, 7 (2006).
- [21] W. F. Vinen, J. Low Temp. Phys. **161**, 419 (2010).
- [22] L. Skrbek, J. Phys.: Conf. Ser. **318**, 012004 (2011).
- [23] M. Tsubota, J. Phys. Soc. Japan **77**, 111006(1 (2008), arXiv:0806.2737.
- [24] M. Tsubota, M. Kobayashi, and H. Takeuchi, Phys. Rep. **522**, 191 (2013), arXiv:1208.0422 [cond-mat.other].
- [25] M. S. Paoletti and D. P. Lathrop, Ann. Rev. Cond. Matt. Phys. **2**, 213 (2011).
- [26] M. S. Paoletti, M. E. Fisher, K. R. Sreenivasan, and D. P. Lathrop, Phys. Rev. Lett. **101**, 154501 (2008), arXiv:0808.1103.
- [27] G. Bewley and K. Sreenivasan, J. Low Temp. Phys. **156**, 84 (2009).
- [28] W. Guo, M. La Mantia, D. P. Lathrop, and S. W. Van Sciver, Proc. Natl. Acad. Sci. U.S.A. **111**, 4653 (2014).
- [29] E. Fonda, D. P. Meichle, N. T. Ouellette, S. Hormoz, and D. P. Lathrop, Proc. Natl. Acad. Sci. U.S.A. **111**, 4707 (2014).
- [30] G. E. Volovik, *The Universe in a Helium Droplet*, The International Series of Monographs on Physics, Vol. 117 (Carendon Press, Oxford, 2003).
- [31] C. N. Weiler, T. W. Neely, D. R. Scherer, A. S. Bradley, M. J. Davis, and B. P. Anderson, Nature **455**, 948 (2008), arXiv:0807.3323 [cond-mat.other].
- [32] E. A. L. Henn, J. A. Seman, G. Roati, K. M. F. Magalhães,

- and V. S. Bagnato, Phys. Rev. Lett. **103**, 045301 (2009), arXiv:0904.2564 [cond-mat.quant-gas].
- [33] A. C. White, C. F. Barenghi, N. P. Proukakis, A. J. Youd, and D. H. Wacks, Phys. Rev. Lett. **104**, 075301 (2010), arXiv:0908.3260 [cond-mat.quant-gas].
- [34] H. Adachi and M. Tsubota, Phys. Rev. B **83**, 132503 (2011), arXiv:1101.0926 [cond-mat.other].
- [35] www.olcf.ornl.gov/computing-resources/titan-cray-xk7.

SUPPLEMENTAL MATERIAL

In this supplement we provide detailed information about the simulations, list of attached movies as well as comparison of the SLDA simulations with the corresponding ETF simulation.

A. Simulation parameters

Simulations are done in a box of size $n_x \times n_y \times n_z$, where $n_x = n_y = 32$ and $n_z = 128$. The simulations contain $N \approx 560$ particles in the following trapping potential:

$$V(x, y, z) = \frac{m}{2}\omega_x^2 x^2 + \frac{m}{2}\omega_y^2 y^2 + \frac{m}{2}\omega_z^2 z^2 + Cy^3,$$

where aspect ratio of the trap $\omega_\perp/\omega_z = 4$ ($\omega_\perp = \sqrt{\omega_x\omega_y}$) is fixed. The remaining trap parameters are characterized by an anisotropy: $\delta = 1 - \omega_y/\omega_x$, and an anharmonicity: C/C_0 , where $C_0 = m\omega_y^2/2R$ and R is Thomas-Fermi radius. The simulation requires to evolve 57,849 two component wave-functions in real time. In order to integrate equations of motion we use a symplectic split-operator method that respects time-reversal symmetry launched on hundreds of GPUs on the Titan supercomputer.

B. Movies – Fermionic Simulations

Movies show paring field profiles (blue surfaces) and location of a vortex (red line) identified as points around which phase of the paring field rotates by 2π .

A.mp4: [<http://youtu.be/Vxv0Ps0s-6s>]
Parameters: $\delta = 9\%$, $C/C_0 = 0\%$.

B.mp4: [<http://youtu.be/gIfhB7QrGxU>]
Parameters: $\delta = 0.5\%$, $C/C_0 = 0\%$.

C.mp4: [<http://youtu.be/7qG03kmN-fs>]
Parameters: $\delta = 9\%$, $C/C_0 = 3\%$.

D.mp4: [<http://youtu.be/K74GUp1cDnM>]
Parameters: $\delta = 0.5\%$, $C/C_0 = 0.15\%$.

E.mp4: [<http://youtu.be/0pg8N91-gZ0>]
Parameters: $\delta = -10\%$, $C/C_0 = 3\%$.

F.mp4: [http://youtu.be/_aW00tI00dw]
Parameters: $\delta = 0\%$, $C/C_0 = 0\%$.
Comment: The edge knife is tilted by angle $\pi/20$ rad.

G.mp4: [<http://youtu.be/utpkynd1Qkc>]
Parameters: $\delta = 0\%$, $C/C_0 = 0\%$.
Comment: Simulation with two edge knives tilted by angle $\pi/20$ rad with different orientation.

H.mp4: [<http://youtu.be/7x1G15TUNQs>]

Parameters: $\delta = 9\%$, $C/C_0 = 3\%$.

Comment: The edge knife is tilted by angle $\pi/20$ rad and rotated in a such way to generate oblique vortex line.

C. Movies – Bosonic Simulations (extended Thomas-Fermi model)

Movies show order parameter $2|\Psi|$ profiles (blue surfaces) and location of a vortex (red line) identified as points around which phase of the order parameter rotates by 2π . Results are obtained using the same lattice parameters as in case of fermionic simulations.

A.ETF.mp4: [<http://youtu.be/uDu00V005D4>]
Parameters: $\delta = 9\%$, $C/C_0 = 0\%$.

B.ETF.mp4: [<http://youtu.be/VUrlvJglqkI>]
Parameters: $\delta = 0.5\%$, $C/C_0 = 0\%$.

C.ETF.mp4: [<http://youtu.be/L50NtMQDfgE>]
Parameters: $\delta = 9\%$, $C/C_0 = 3\%$.

D.ETF.mp4: [<http://youtu.be/H0IB-R1TwJU>]
Parameters: $\delta = 0.5\%$, $C/C_0 = 0.15\%$.

E.ETF.mp4: [<http://youtu.be/EXL01BbsKS8>]
Parameters: $\delta = -10\%$, $C/C_0 = 3\%$.

D. Simulation of Quantum Turbulence

The simulation of quantum turbulence was done with lattice $48 \times 48 \times 128$, and particle number $N = 1410$. The confining potential is axially symmetric ($\delta = 0\%$) with aspect ratio $\omega_\perp/\omega_z = 2.67$. There is no anharmonicity term ($C/C_0 = 0\%$). Number of two component wave-functions to be evolved in real time is 131,629 and to integrate equations of motion we used 2048 Titan's GPUs. As the stirrers we used repulsive Gaussian potentials of width 1.25 of lattice spacing and amplitude $0.75\varepsilon_F$. We provide two movies:

QT.mp4: [<http://youtu.be/nCGtq8k6SAQ>]
Dynamics of the cloud showing paring field profiles (blue surfaces).

E. Comparison of Fermionic and Bosonic Simulations

On the next page we compare the SLDA simulations presented in the main body of the paper (top of each figure) with the corresponding ETF simulation with the same initial conditions and preparation.

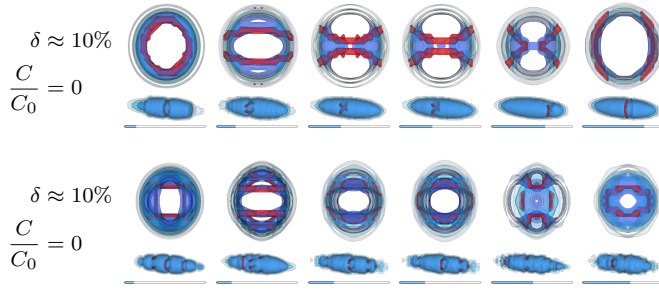


FIG. 6. (Color online, click on frames to view movie online.) ETF analogue of the SLDA simulation in the top of Fig. 2

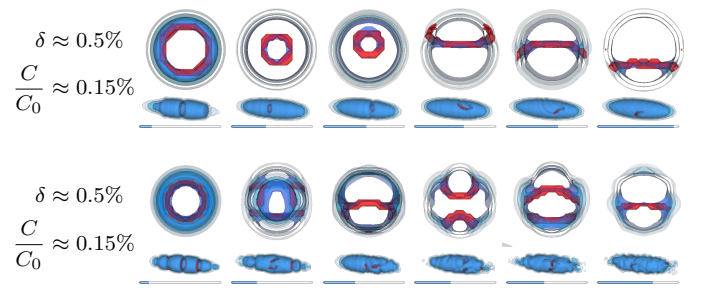


FIG. 9. (Color online, click on frames to view movie online.) ETF analogue of the SLDA simulation in the bottom of Fig. 3

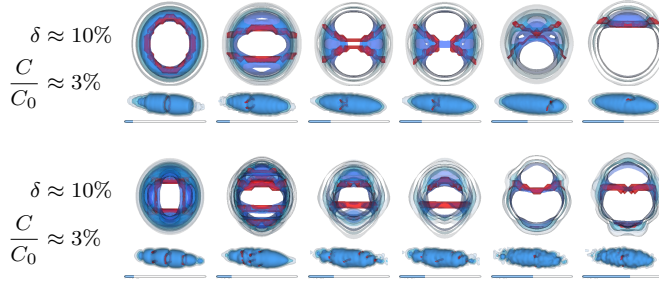


FIG. 7. (Color online, click on frames to view movie online.) ETF analogue of the SLDA simulation in the bottom of Fig. 2

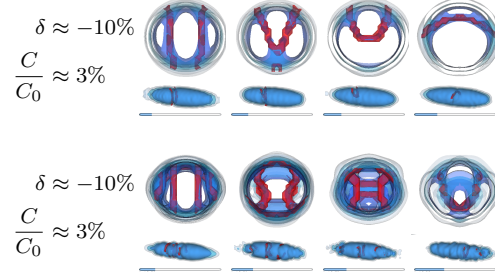


FIG. 10. (Color online, click on frames to view movie online.) ETF analogue of the SLDA simulation in the top of Fig. 4

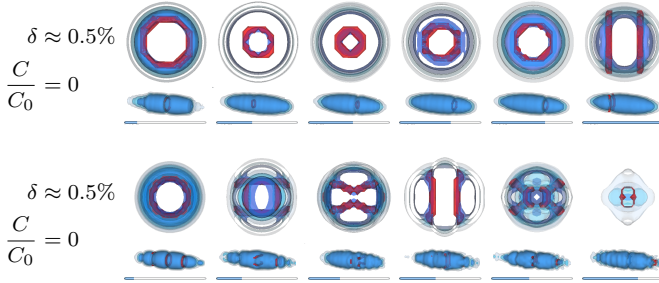


FIG. 8. (Color online, click on frames to view movie online.) ETF analogue of the SLDA simulation in the top of Fig. 3